IMECE2025-168114

PHYSICS-BASED PREDICTION OF REMAINING USEFUL LIFE OF LITHIUM-ION BATTERIES IN FUEL CELL-BATTERY HYBRID AIRCRAFT USING AN OPEN-SOURCE MODELICA FRAMEWORK

Nathaniel Cooper¹, Ali Mahboub Rad^{2,3}, Korebami Adebajo¹, Austin R.J. Downey^{1,4}, Jie Zhang^{2,3}

Department of Mechanical Engineering, University of South Carolina, Columbia, SC
 Department of Electrical and Computer Engineering, University of Texas at Dallas, Richardson, TX
 Department of Mechanical Engineering, University of Texas at Dallas, Richardson, TX
 Department of Civil Engineering, University of South Carolina, Columbia, SC

ABSTRACT

One alternative to all-electric powertrains in the aviation industry is the introduction of hybrid fuel cell/battery architectures. Vital to the operation of such a system is the development of effective energy management systems to manage load sharing and component health. In particular, an extension of battery service life is a priority as this is the component expected to be replaced most frequently. A framework for developing a robust energy management system has been built within the open-source framework of the OpenModelica multi-physics libraries, including a simplified fuel cell, battery stack, hydrogen storage tank, and customizable flight generator. Initial results indicated two main focuses for this study. First, the handling of high-power periods, such as takeoff, dominates the battery's discharge profile. In particular, batteries repeatedly subjected to strain from takeoff due to a string of short-range, 45-minute flights experience a service life of less than half (300 flight hours) that of long-range, 120-minute flights (700 flight hours). Secondly, it was shown that small fluctuations in power demand can result in large reductions of service life up to 20% of the ideal, making their management a key concern.

1. INTRODUCTION

Electric aircraft are a potential solution to the challenges of sustainable transportation, with reduced carbon emissions, lower noise levels, and improved mechanical efficiency. Battery lifespan has emerged as a key factor in the economics [1]. However, fast charge cycles are required to maintain availability [2], which, combined with the high power demand in flight, leads stacks to rapidly deteriorate [3].

Hydrogen fuel cell/battery hybrid architectures have been frequently proposed as an alternative to all-electric systems in land-based transportation. For example, Fragiacomo [4] and Baumann [5] have proposed layouts similar to that depicted in Fig. 1 for land vehicles. In this case, the PEM fuel cell acts

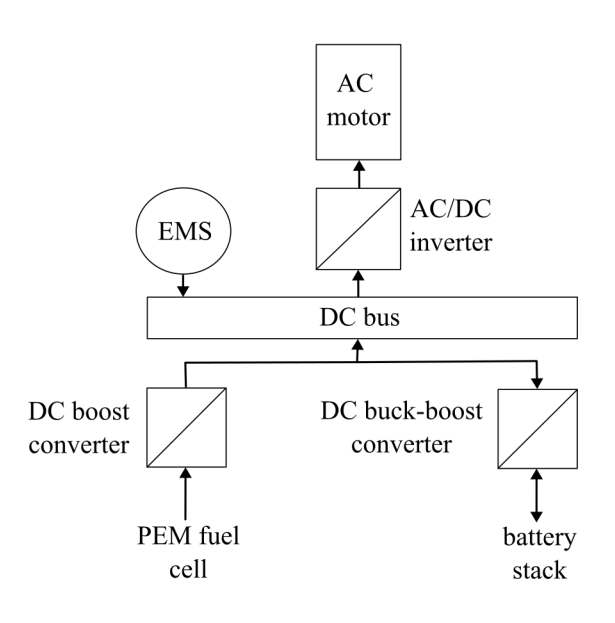


FIGURE 1: LAYOUT OF A PROPOSED POWER TRAIN FOR FUEL CELL-BATTERY HYBRID VEHICLES.

as the primary power supply for the vehicle, outputting a nearconstant load. The battery supplements this by supplying load during short-term transients and high-power applications. The concept can be further extended by integrating supercapacitor banks [4–7] to enhance transient responses. In principle, these architectures can be easily ported to aircraft [8, 9], potentially even in concert with turbogenerators and other traditional methods. However, management of the battery's lifespan remains essential. Compare, for example, the battery stacks of the Velis Electro, a small, all-electric, battery-powered trainer aircraft manufactured by Pipistrel, which are estimated to need overhaul after 500 flight hours [10, 11], to the lifespan of the average fuel cell of over 4000 operating hours [12]. Batteries thus represent a major bottleneck in the maintenance cycle.

The energy management system (EMS) is key to the performance of hybrid systems as it balances demand across each of the separate power supplies efficiently and safely. EMS approaches are varied, including operation mode control, equivalent consumption minimization, fuzzy logic, predictive controls, and traditional PIs [13]. At present, only a small handful of studies demonstrate control on physical hardware [14, 15], with the vast majority of work being conducted in simulation using tools such as MATLAB/SIMULINK [16–18], a proprietary resource requiring a license to utilize.

Modelica is an open-source, object-oriented language designed for multi-domain modeling of complex physical systems, making it particularly suitable for simulating complicated electromechanical systems [19]. While its capabilities have been explored in modeling electric aircraft, this application is still in its nascent stage, and mature, robust libraries specifically tailored for electric aircraft are yet to be fully developed. Prior works have positively demonstrated Modelica's potential in this domain: Bals et al. [20] presented new modeling and simulation methods for electric aircraft systems, including optimization of electric network architecture and system integration using virtual testing; Podlaski et al. [21] took initial steps in modeling fully electrified propulsion systems for aircraft using Modelica, introducing novel multi-domain components; and Castro et al. [22] developed Modelica models to assess the dynamic performance of different turboelectric architectures for electrified powertrains. Prior work by the authors in Cooper et al. [11] used Modelica to model the power system of an all-electric aircraft based on the Pipistrel Velis Electro to show that advanced controls could be leveraged to extend battery life with up to a 50% increase in flight time in the best case. These studies collectively demonstrate the potential of Modelica in modeling electric aircraft systems, highlighting its usefulness while also underscoring the need for more mature libraries to fully support the complexity of electric aircraft modeling.

The object of the present work is the development of a basis for an EMS library written for the Modelica language, using the standard multi-physics libraries provided by OpenModelica [23]. A representative test case based on regional flights using a hybrid fuel cell and lithium-ion battery system is explored to demonstrate the framework's capabilities and assess the impact of power management strategies on battery degradation. Code for the considered example problem is provided through a public repository [24]. Moreover, the developed open-source library is also available through a publicly shared repository [25]. The contributions of this paper are twofold. First, this paper contributes a publicly accessible OpenModelica-based simulation environment for hybrid hydrogen fuel cell and battery architectures. Second, a detailed case study quantifying the impact of flight scheduling and power fluctuation on lithium-ion battery degradation in aircraft. The open-source framework is intended to support further research in energy management systems (EMS) design and battery prognostics for electrified aviation.

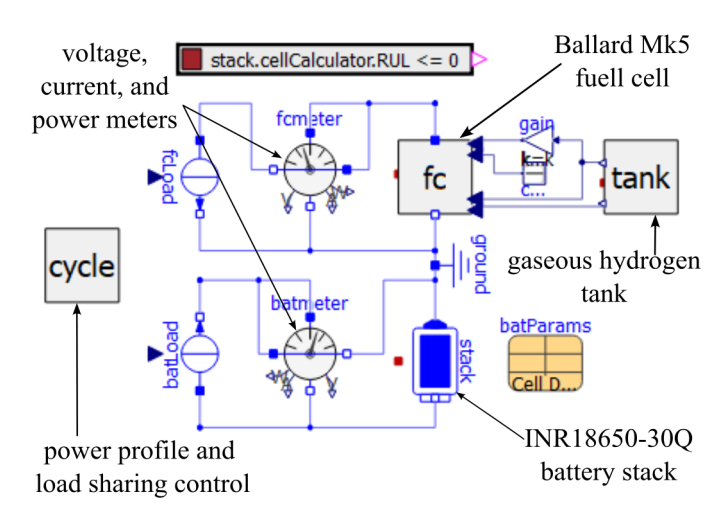


FIGURE 2: THE SIMPLIFIED POWER SUPPLY MODEL IN OPEN-MODELICA.

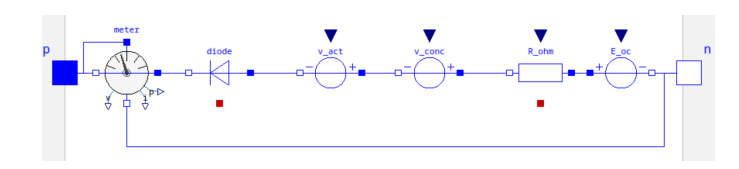


FIGURE 3: EQUIVALENT CIRCUIT MODEL OF A SIMPLE FUEL CELL.

2. METHODOLOGY

This section describes the methodology utilized by this work in modeling the considered hybrid Hydrogen fuel cell and battery architecture.

2.1. System-level Architecture Modeling.

The object of the present work is the development of a basis for an EMS library written for the Modelica language, using the standard multi-physics libraries provided by OpenModelica [23]. A simplified model of a hybrid fuel cell/battery power supply, as pictured in Fig. 2. taken from the literature and experimental battery characterization data. The "fc" block (2.2) consists of a combination of theoretical and empirical relations necessary for describing the behaviour of a Ballard Mk5 fuel cell, fed with hydrogen by the "tank" (2.2.6) block. The "stack" is a modified version of the OpenModelica standard library's model, incorporating a degradation model and characterized by experimental data (2.3). The "cycle" block combines the power profile generator and load sharing agent (2.4); a generic flight power profile is then developed for a Cessna 206 using publicly available data to characterize short distance flights around the southeastern United States and applied to the simplified power supply via a rudimentary load sharing agent. Combined, these blocks can simulate any number of flights of any length and provide a basis for the study of the battery stack's degradation over time.

2.2. Modeling of a Simple Fuel Cell

A single hydrogen fuel cell can be modeled using a simple equivalent circuit model, as pictured in Fig. 3. Each component

represents a specific phenomenon in the internal dynamics of the cell; the particulars of each are described in the subsections below. When combined in series, they describe the total voltage of a fuel cell [26, 27]

$$E = NN_m(E_{\rm OC} + V_{\rm act} + V_{\rm conc} + V_{\rm ohm}), \tag{1}$$

where $E_{\rm OC}$ is the open circuit voltage, $V_{\rm act}$ is the activation losses, $V_{\rm conc}$ is the concentration losses, $V_{\rm ohm}$ is the ohmic losses, N_m is the number of fuel cell modules and N is the number of cells per module. Note that the direction of the pins for $V_{\rm act}$, $V_{\rm conc}$, $V_{\rm ohm}$ are opposite that of $E_{\rm OC}$; they therefore represent voltage *losses* rather than gains.

2.2.1. Open-Circuit Voltage E_{OC} In general, for any electrochemical cell, the open circuit voltage E_{OC} is defined by [26]

$$E_{\rm OC} = \frac{\Delta G_{\rm react}}{nF},\tag{2}$$

where ΔG_{react} is the free energy change for the reaction, n is the number of electrons transferred in the reaction, and F is the Faraday constant. For a basic fuel cell, the global and half reactions are given in Eq. [26], which gives a value of n = 2. Generally speaking, air is provided as an oxidant rather than pure oxygen.

Anode : $2H_2 \to 4H^+ + 4e^-$

Cathode : $O_2 + 4H^+ + 4e^- \rightarrow 2H_2O$

Overall : $2H_2 + O_2 \rightarrow 2H_2O$

 ΔG_{react} can further be split into two terms to adjust for reactions taking place at non-standard temperature and pressures, giving the final expression For a basic hydrogen fuel cell, this will be [26, 28]

$$E_{\rm OC} = \frac{1}{nF} \left(\Delta G_{\rm react}^{\circ} + RT ln \left(\frac{P_{\rm H_2} P O_2^{0.5}}{P_{\rm H_2 O}} \right) \right). \tag{3}$$

2.2.2. Activation Losses V_{act} The activation losses represented by V_{act} are driven by the need to physically transport electrons between the anode and cathode. To do so, some of the energy released by the overall cell reaction is wasted, resulting in a slight voltage loss. In general, these losses are given by [26, 27]:

$$V_{\text{act}} = a \ln \left(\frac{i}{i_0} \right). \tag{4}$$

In Eq. 4, i is the current area density (A/cm²) and i_0 is a parameter called the exchange current density. The equation holds only if $i > i_0$ [26]; if the cell current falls below this threshold, the activation losses are negligible. Many sources split the logarithm into a constant term, characterized by i_0 , and a non-constant term characterized by i. The former can then be shifted and incorporated into the open circuit voltage term, leaving a simple expression for the activation losses [27]

$$V_{\rm act} = a \ln i. ag{5}$$

TABLE 1: PARAMETERIZATION OF A BALLARD MK5 FUEL CELL

parameter	expression
<i>a</i> (V)	$4.01\times10^{-2} - 1.40x\times10^{-4} T$
m(V)	$3.3\times10^{-3} - 8.2\times10^{-5} T$
$b (cm^2 \cdot mA^{-1})$	8×10^{-3}
$r (k\Omega \cdot cm^2)$	$4.77 \times 10^{-4} - 3.32 \times 10^{-6} T$

2.2.3. Concentration Losses V_{conc} The concentration losses stem from an effective shortage of reactant at the electrodes. In effect, the actual, local concentration of a reactant on the electrode surface is actually slightly lower than the idealized amount assumed by Eq. 3. The voltage produced is therefore slightly lower than what would otherwise be predicted, and V_{conc} characterizes this loss. The concentration voltage drop is described in Eq. 6 below [26]; the parameter i_{lim} is the limiting current density and is the cell current produced when the reactant is supplied at the maximum, ideal rate

$$V_{\rm conc} = \frac{RT}{nF} \ln \left(\frac{i_{\rm lim} - i}{i_{\rm lim}} \right). \tag{6}$$

Alternatively, the purely empirical relation 7 [26, 27, 29] has been shown to give an excellent fit to experimental results;

$$V_{\rm conc} = me^{bi}. (7)$$

2.2.4. Ohmic Losses V_{ohm} The ohmic losses are caused by the internal resistance of the cell, and are given by Ohm's Law [26–28]. Note that because *i* is given in A/cm², the resistance *r* must be given in $k\Omega$ -cm²,

$$V_{\text{ohm}} = ri. (8)$$

2.2.5. Fuel Cell Parameterization The overvoltages given by Eq. 5, Eq. 7, and 8 require a total of five parameters to fully characterize the cell: a, m, b, r, and the active area of the cell A. A set of empirical relations developed for a Ballard MK5 cell (active area 232 cm²) is used to characterize these [27], summarized in Table 1. Note (1) that all temperatures are assumed to be in degrees Celsius rather than Kelvin and (2) that in the simulation the cell is assumed to operate at a constant 30° C.

2.2.6. Fuel Supply System In addition to the above, a fuel supply system is also required to complete the model. The partial pressures in Eq. 3 are given, in bars, by [28]

$$P_{\rm H2} = (1 - U_{\rm H2}) x_{\rm H2} P_{\rm fuel},$$
 (9a)

$$P_{O2} = (1 - U_{O2}) x_{O2} P_{air}$$
, and (9b)

$$P_{\text{H2O}} = (x_{\text{H2O}} + 2x_{\text{O2}}U_{\text{O2}}) P_{\text{air}}.$$
 (9c)

In Eqs. 9a through 9c, $U_{\rm H2}$ and $U_{\rm O2}$ represent the utilization rate of the gases provided to the cell, while each x represents its constituents' concentration. The utilization rates are defined as [26, 28]

$$U_{O2} = \frac{IRT}{2nFP_{\text{air}}Q_{\text{air}}x_{O2}}$$
 (10a)

TABLE 2: MANUFACTURER SPECIFICATIONS OF AN INR 18650-30Q.

specification	Samsung 30Q
diameter (mm)	18.33
length (mm)	64.85
weight (g)	48.0
cell capacity (A-hr)	3.0
nominal voltage (V)	3.600
standard charge method	CCCV
standard charge current (A)	1.5
standard charge voltage (V)	4.2
standard charge cutoff (mA)	150
maximum charge current (A)	4.000
standard discharge cutoff voltage (V)	2.5
maximum continuous discharge current (A)	15.0
operating temperature (°C)	-20 to 75

$$U_{H2} = \frac{IRT}{nFP_{\text{fuel}}Q_{\text{fuel}}x_{\text{H2}}},\tag{10b}$$

where I is the current (not current density) produced by the cell and P (in bars) and Q (in m^3/s) are the supply pressure and volumetric flow rate of the air and fuel streams, respectively. Hydrogen is supplied to the system via a simple tank maintained at a constant temperature and pressure, with ideal gas behavior assumed. The flow rate out of the tank and into the fuel cell is controlled by a pressure regulator and defined by (again, with pressures in bars) [30]:

$$Q_{\text{fuel}} = \frac{0.0004734C_v P_{\text{tank}}}{\rho_{\text{tank}}} \sqrt{\frac{(P_{\text{tank}} - P_{\text{fuel}}) M}{T_{\text{tank}} P_{\text{tank}} Z}}.$$
 (11)

Here, Z is the compressibility factor (assumed to be 1) and M is the molar mass of the gas (2.016 g/mol for H₂). The flow coefficient is determined by extensive manufacturer testing and is generally provided on the product data sheet; it is up to the user to choose a coefficient and regulator that will provide appropriate flow for their application. After some trial and error, it was found that a value of C_{ν} =0.6 was sufficient to provide the appropriate current and power in the cell. Air was provided as an oxidant at atmospheric pressure and at three times the flow rate of hydrogen.

2.3. Modeling of the Battery Stack

The battery stacks in this study are based on the INR 18650-30Q, a graphite anode, LiCo₂ cathode cell manufactured by Samsung. Key manufacturer specifications of the cell are summarized in Table 2 [31]. Testing of single cells was performed at the University of South Carolina's Adaptive Real-Time Systems (ARTS) Lab on an NHR 9200 battery system controlled by a programmable LabVIEW system.

2.3.1. SOC-OCV Curve and Internal Resistance The SOC-OCV curve maps the open circuit voltage (OCV) of a cell to its state of charge (SOC) and governs the measured cell voltage as it is charged and discharged. To characterize this, a series of short, 6 A pulses was applied to a single cell,

discharging it in increments of 10% SOC. Then, all current load was removed, and the cell voltage was allowed to settle, thereby establishing the OCV at each incremental SOC. The data for these tests is available through a public repository [32]. The resulting measurements were then curve fit using a least-squares method to a function of the form [33]:

$$OCV = K_0 + K_1 SOC + K_2 \ln(SOC) + K_3 \ln(1 - SOC)$$
 (12)

At 20 degrees Celsius, these coefficients were $K_0 = 3.284$, $K_1 = 0.823$, $K_2 = 0.0959$, and $K_3 = 0.00343$. The cell's internal resistance was estimated by measuring the voltage drop during each pulse of the above tests and calculating the resistance from Ohm's Law. At 20 °C, this was found to be 0.0162 Ω .

2.3.2. Degradation Model In addition, an empirical model from the literature was implemented to describe the capacity fade of the cell with repeated use. The model computes the cell's current capacity as a function of its nominal capacity (C_0), mean SOC (SOC_m), depth of discharge (DOD), and equivalent full cycles (EFC) and takes the form [34]

$$C = \frac{AC_0}{100} \left(\frac{EFC}{100}\right)^b,\tag{13}$$

where

$$A = 3.25SOC_m \left(100 + 3.25DOD - 2.25DOD^2 \right). \tag{14}$$

To check the accuracy of this model, a simulated benchmark test was performed. Per the 30Q datasheet, after 250 cycles, a cell should have a capacity of $0.6C_0$ when cycled continuously at the nominal 1.5 A charge rate and a maximum 15 A discharge rate. Under these conditions, the simulated cell's final capacity was estimated to be $0.6036C_0$, precisely as described by the datasheet. The above equations were thus deemed sufficient to model battery cell degradation.

2.4. Development of a Generic Flight Profile and the Load Sharing Agent

A generic power profile was developed to determine the load at any particular time in flight. This consists of three phases, illustrated in Fig. 4: (1) pre/post-flight taxing, (2) takeoff, and (3) cruise. To facilitate this in simulation, the fully customizable "cycle" block of Fig. 2 was implemented. The block allows users to define all the various parameters of the flight, including taxi power (P_{taxi}), maximum power during takeoff (P_{max}), cruise power (P_{cruise}), the duration of each phase (t_{taxi} , t_{max} , and t_{cruise}), and the time needed to ramp to or from each phase (t_{taxiRamp} and t_{maxRamp}). It is assumed that the same time is taken to ramp down from maximum to cruise power, and from cruise power to taxi power, as it is to ramp up from taxi to maximum power during takeoff. At the end of each flight, a short rest period is observed to recharge the battery and replace the hydrogen tanks.

TABLE 3: APPROXIMATED FLIGHT PROFILE PARAMETERS FOR REGIONAL SOUTHEASTERN FLIGHTS

route	P _{taxi} (kW)	ttaxi (min)	P _{max} (kW)	t _{max} (min)	P _{cruise} (kW)	t _{cruise} (min)
Charlotte/Myrtle Beach	30	12	190	12	160	47
Columbia/Richmond 1	55	14	230	2	170	104
Columbia/Richmond 2	40	7.3	200	20	125	120
Columbia/Richmond 3	30	6	225	2	165	110
Greenville/Augusta	50	10	215	3	150	45
average	41	9.86	212	7.8	154	85.2

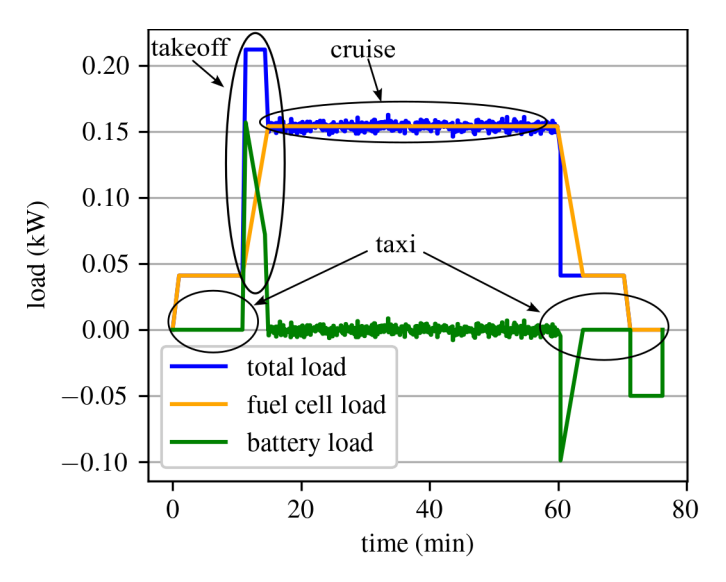


FIGURE 4: A GENERIC FLIGHT POWER PROFILE.

2.4.1. Determination of Flight Parameters Data on power curves for various flights were gathered from fuel consumption records sourced from publicly available flight data [35]. For each flight, the consumption rate was multiplied by the specific energy and density of the fuel (43.5 MJ/kg and 721.1 kg/m³ [36], respectively, for 100LLV fuel) to determine the power generated by the combustion of the fuel. By considering the engine's efficiency at different times, this energy was then converted into usable power for the aircraft. For taxi, cruise, and descent phases, efficiency was assumed to be 30%, whereas, during takeoff, it was set at 19%, as engines generally operate less efficiently at high power demands like takeoff.

In the end, a small selection of five flights was chosen to characterize the generic power profile. A summary of the approximate pertinent parameters for these flights is given in Table 3, along with the average values used to parameterize the simulation. The time taken to ramp to and from maximum power was somewhat inconsistent from flight to flight, with 30 seconds judged to be a representative duration. Finally, it was assumed that 60 seconds was spent immediately before and after each flight to ramp to and from taxi power.

2.4.2. Load Sharing A simple load-sharing scheme is shown in algorithm 1 and is as follows. In general, the aircraft is considered to pull from the fuel cell as its primary power supply. Thus, during the majority of the flight, the fuel cell receives the full load. However, during transient periods, the total

Algorithm 1 SIMPLIFIED LOAD SHARING SCHEME FOR THE CONSIDERED HYBRID AIRCRAFT CONSIDERED.

```
1: for each time step do
       if Takeoff then
3:
           FuelCellPower ← slowly ramp to CruisePower
           BatteryPower \leftarrow TotalDemand - FuelCellPower
4:
5:
       else if Cruise then
           Noise ~ random normal fluctuation
6:
           EffectiveDemand ← CruisePower + Noise
7:
           if EffectiveDemand > CruisePower then
8:
               Battery discharges to meet extra demand
9:
10:
           else
11:
               Fuel cell charges battery with excess power
           end if
12:
       else if Landing then
13.
           FuelCellPower ← slowly ramp down
14:
           BatteryPower ← FuelCellPower – TotalDemand
15:
16:
       else
17:
           FuelCellPower ← TotalDemand
           BatteryPower \leftarrow 0
18:
       end if
19.
20: end for
```

load and fuel cell load diverge. For example, during takeoff, the fuel cell slowly ramps up to cruise power, rather than swiftly up to maximum power and back. The difference required to complete takeoff is supplied by the battery, as illustrated in Fig. 4. Similarly, during landing, the fuel cell ramps down more slowly than the total power demand of the aircraft, with the extra power produced being routed to charge the battery. To simulate the slight variations observed in the power profile of real flights, a noise generator was applied during cruise using a normal distribution with a standard deviation of 2.109 kW. When the signal generated is greater than the cruise power of 154 kW, the battery partially discharges to meet demand; when the signal is less than 154 kW, the fuel cell instead partially charges the battery. These charges and discharges, although tiny on an individual basis, add up over the course of a flight to increase the total equivalent cycles experienced by the stack and degrade it.

2.4.3. Sizing the Fuel Cell and Battery Stacks As seen in Table 3, the fuel cell stack must be able to supply a minimum of 142 kW of constant power while remaining below the maximum current density of ~450 mA/cm² for the Ballard MK5. A short calculation indicates that 8 modules consisting of 300 cells each would be sufficient for this purpose. The battery stack was

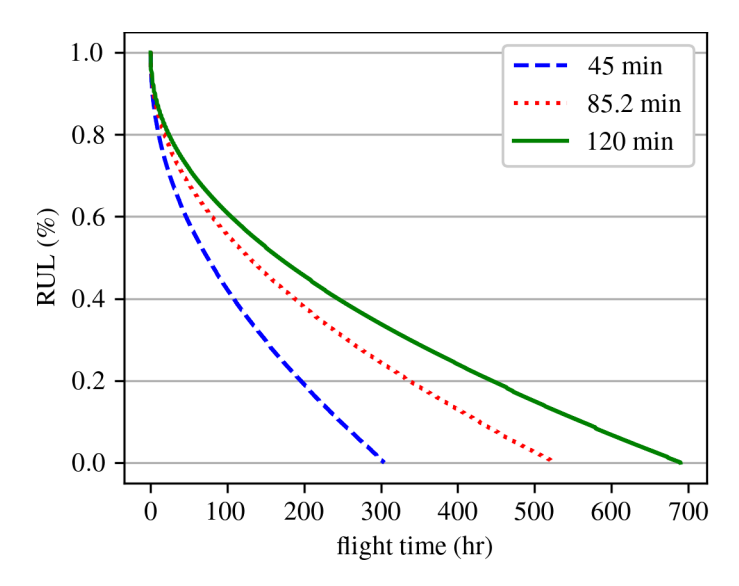


FIGURE 5: BATTERY REMAINING USEFUL LIFE AS A FUNCTION OF FLIGHT HOURS.

similarly sized with the constraint that it must act as the aircraft's emergency power supply. It must therefore have enough capacity to fly the plane under cruise power for a minimum of thirty minutes. It was estimated that four stacks mounted in parallel in a 168-series, 12-parallel configuration can supply the necessary power for $\sim \! 30$ minutes. In addition, it was calculated that this stack can supply a maximum power of 435 kW, more than enough to complete takeoff should the fuel cell fail to ramp.

3. RESULTS AND DISCUSSION

In general, batteries are considered to reach their end of life when their capacity reaches 80% of their initial, nominal capacity; for an INR18650-30Q, this would equate to 2.4 Ah. A commonly used measure of battery health is remaining useful life (RUL), defined as the percentage of capacity fade remaining before disposal. Figure 5 plots the RUL of the 30Q stack against the total flight hours for three different cruise lengths, 45 minutes (the minimum time in Table 3), 85.2 minutes (the average value), and 120 minutes (the maximum value). One immediate observation from this figure is that battery lifespan is inversely related to the number of flight hours; the longer the flight, the longer the battery stack will last. In fact, stacks subjected to short, 45minute flights logged only 300 flight hours before replacement, less than half that of the 700 hours of long-range 120-minute flights. Intermediate, 85.2-minute flights fell between the two extremes, recording approximately 540 hours.

This may seem counterintuitive, but is easily explainable when one examines the power profile in Fig. 4. In every flight, the deepest and most stressful discharge occurs during takeoff; the numerous small charges and discharges occurring to noise in the power profile during cruise are minuscule, even in aggregate, when compared to the initial discharge. Limiting an aircraft to repeated short-range flights means the battery will experience this stress more often than engaging in medium- and long-range flights. In every case, the battery reaches its end of life after approximately the same number of equivalent cycles, but be-

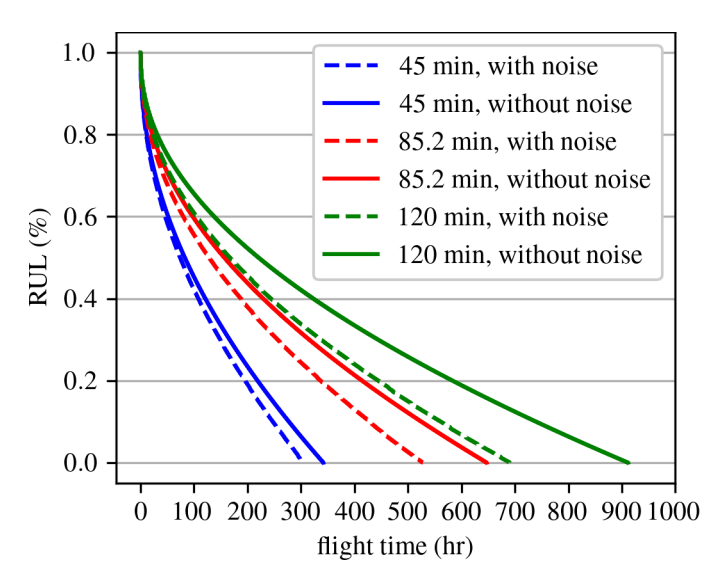


FIGURE 6: IMPACT OF NOISE IN THE POWER PROFILE DURING CRUISE ON BATTERY RUL.

cause the short-range case experiences takeoff more often, it also reaches this limit sooner.

However, this is not to say that the noise in the load profile has no effect whatsoever. Fig. 6 plots the stack RUL for the same three cruise periods (1) with the noise generator and (2) without. In every case, battery lifespan is reduced, up to a factor of over 20% in the case of 120-minute flights. On an individual flight basis, battery stress induced by takeoff dominates, but in the long term, small fluctuations in demand still have a substantial effect.

These findings imply two foci for any EMS. First, an optimal strategy for managing takeoffs is essential, as this is the primary driver for battery degradation. Secondly, a way must be found to effectively manage small fluctuations in demand throughout the life of the stack. Incorporation of ultracapacitors into the system may be one way to manage these issues, especially the latter; their high charge and discharge rate can help smooth the power curve and reduce the aggregate strain on the battery in the long term. In addition, it will be vital for airline planners to manage and plan their logistics accordingly to avoid overscheduling short-range flights, which stress the stack through repeated takeoffs.

4. CONCLUSIONS

Energy management of fuel cell/battery hybrid architectures is an ongoing field of research in the push for electrifying transportation. This work aims to provide a basis for modeling these systems in an open-source environment that can be easily shared and modified. The application of a rudimentary load-sharing agent to the system indicated two key areas of concern in managing battery health: the handling of high-power periods, such as takeoff, and the slow accumulation of stress over time due to small fluctuations of the load.

Limitations still remain. First and foremost, thermal management must be considered. This is especially important due to the risk of thermal runaway in the battery stack, an especially catastrophic outcome in the aviation industry [37]. Rather than assuming a constant operating temperature for all components, the disposal of waste heat and energy required to operate cooling

systems must be accounted for. The storage tank also requires some energy input to maintain its temperature and pressure, which may be partially supplied by waste heat or by an electric heater. In addition, aircraft have numerous small electronic systems operating at all times, which will also draw a small amount of power. Finally, the power profiles used here are somewhat idealized, with no aborted takeoffs or landings and no minor ascents or descents during cruise. These irregularities introduce strains comparable to those during takeoff and must be addressed.

ACKNOWLEDGMENTS

This material is partially supported by the Air Force Office of Scientific Research (AFOSR) through award no. FA9550-21-1-0083. Additional funding for this work comes from the National Science Foundation (NSF) grant numbers CPS - 2237696. This project is also partially supported by the University of South Carolina Office of Undergraduate Research through the Magellan Scholar Program. Any opinions, findings, conclusions, or recommendations expressed in this material are those of the authors and do not necessarily reflect the views of the National Science Foundation, the United States Air Force, or the University of South Carolina.

REFERENCES

- [1] Yang, Xiao-Guang, Liu, Teng, Ge, Shanhai, Rountree, Eric and Wang, Chao-Yang. "Challenges and key requirements of batteries for electric vertical takeoff and landing aircraft." *Joule* Vol. 5 No. 7 (2021): pp. 1644–1659. DOI 10.1016/j.joule.2021.05.001.
- [2] Adebajo, Korebami, Anthony, George, Peskar, Jarett, Downey, Austin R., Chen, Yuche and Hu, Chao. "Impact of Charging Rate and State of Charge on Electric Aircraft Battery Degradation Using a Multi-Domain Model With Realistic Southeastern U.S. Flight Paths." AIAA SCITECH 2025 Forum. 2025. American Institute of Aeronautics and Astronautics. DOI 10.2514/6.2025-2705.
- [3] Justin, Cedric Y., Payan, Alexia P., Briceno, Simon I., German, Brian J. and Mavris, Dimitri N. "Power optimized battery swap and recharge strategies for electric aircraft operations." *Transportation Research Part C: Emerging Technologies* Vol. 115 (2020): p. 102605. DOI 10.1016/j.trc.2020.02.027.
- [4] Fragiacomo, Petronilla, Genovese, Matteo, Piraino, Francesco, Corigliano, Orlando and De Lorenzo, Giuseppe. "Hydrogen-Fuel Cell Hybrid Powertrain: Conceptual Layouts and Current Applications." *Machines* Vol. 10 No. 12 (2022): pp. 1121–1140. DOI 10.3390/machines10121121.
- [5] Bauman, Jennifer and Kazerani, Mehrdad. "A Comparative Study of Fuel-Cell–Battery, Fuel-Cell–Ultracapacitor, and Fuel-Cell–Battery–Ultracapacitor Vehicles." *IEEE Transactions on Vehicular Technology* Vol. 57 No. 2 (2008): pp. 760–769. DOI 10.1109/TVT.2007.906379.
- [6] Jia, Junbo, Wang, Gucheng, Cham, Yew Thean, Wang, Youyi and Han, Ming. "Electrical Characteristic Study of a Hybrid PEMFC and Ultracapacitor System." *IEEE Transactions on Industrial Electronics* Vol. 57 No. 6 (2010): pp. 1945–1953. DOI 10.1109/TIE.2009.2022066.

- [7] Do, Tri Cuong, Truong, Hoai Vu Anh, Dao, Hoang Vu, Cong, Minh Ho, To, Xuan Dinh, Dang, Tri Dung and Ahn, Kyoung Kwan. "Energy Management Strategy of a PEM Fuel Cell Excavator with a Supercapacitor/Battery Hybrid Power Source." *Energies* Vol. 12 No. 22 (2019): pp. 24362–4386. DOI 10.3390/en12224362.
- [8] Gao, Yuan, Jausseme, Charles, Huang, Zhen and Yang, Tao. "Hydrogen-Powered Aircraft: Hydrogen-electric hybrid propulsion for aviation." *IEEE Electrification Magazine* Vol. 10 No. 2 (2022): pp. 17–26. DOI 10.1109/MELE.2022.3165725.
- [9] Bradley, Marty. "Identification and Descriptions of Fuel Cell Architectures for Aircraft Applications." 2022 IEEE Transportation Electrification Conference and Expo: pp. 1047–1050. 2022. Institute of Electrical and Electronics Engineers.
- [10] Pipistrel Vertical Solutions d.o.o. *Velis Electro Pilot's Operating Handbook*, Version B00 (2020).
- [11] Cooper, Nathaniel, Anthony, George, Peskar, Jarett, Downey, Austin R. and Booth, Kristen. "Data Assimilation in a Modelica Framework for Optimizing Battery Longevity in Electric Aircraft." AIAA SCITECH 2025 Forum. 2025. American Institute of Aeronautics and Astronautics. DOI 10.2514/6.2025-2706.
- [12] Benjamin, Tom, Borup, Rod, Garland, Nancy, Gittleman, Craig, Habibzadeh, Bahman, Hirano, Shinichi, Ho, Donna, Kleen, Greg, Kopasz, John, Lakshmanan, Balsu, Masten, David, Mehall, Mark, Myers, Deborah, Onorato, Shaun, Papageorgopoulo, Dimitrios, Peterson, David, Spendelow, Jacob, Waldecker, Jim, Wilson, Adria and Zou, Max. "US-Drive Fuel Cell Technical Team Roadmap." (2017).
- [13] García, Pablo, Torreglosa, Juan P., Fernández, Luis M. and Jurado, Francisco. "Control strategies for high-power electric vehicles powered by hydrogen fuel cell, battery and supercapacitor." Expert Systems with Applications Vol. 40 No. 12 (2013): pp. 4791–4804. DOI https://doi.org/10.1016/j.eswa.2013.02.028. URL https://www.sciencedirect.com/science/article/pii/S0957417413001449.
- [14] Şefkat, Gürsel and Özel, Mert Ali. "Experimental and numerical study of energy and thermal management system for a hydrogen fuel cell-battery hybrid electric vehicle." *Energy* Vol. 238 (2022): p. 121794. DOI https://doi.org/10.1016/j.energy.2021.121794. URL https://www.sciencedirect.com/science/article/pii/S0360544221020429.
- [15] Solano Martinez, Javier, Hissel, Daniel, Pera, Marie-Cécile and Amiet, Michel. "Practical Control Structure and Energy Management of a Testbed Hybrid Electric Vehicle." *IEEE Transactions on Vehicular Technology* Vol. 60 No. 9 (2011): pp. 4139–4152. DOI 10.1109/TVT.2011.2169821.
- [16] Ahmadi, Saman, Bathaee, S.M.T. and Hosseinpour, Amir H. "Improving fuel economy and performance of a fuel-cell hybrid electric vehicle (fuel-cell, battery, and ultra-capacitor) using optimized energy management strategy." *Energy Conversion and Management* Vol. 160 (2018): pp. 74–84. DOI https://doi.org/10.1016/j.enconman.2018.01.020.

- URL https://www.sciencedirect.com/science/article/pii/S0196890418300207.
- [17] Hannan, M.A., Azidin, F.A. and Mohamed, A. "Multi-sources model and control algorithm of an energy management system for light electric vehicles." *Energy Conversion and Management* Vol. 62 (2012): pp. 123–130. DOI https://doi.org/10.1016/j.enconman.2012.04.001. URL https://www.sciencedirect.com/science/article/pii/S0196890412001835.
- [18] Gherairi, Salsabil. "Hybrid Electric Vehicle: Design and Control of a Hybrid System (Fuel Cell/Battery/Ultra-Capacitor) Supplied by Hydrogen." *Energies* Vol. 12 No. 7 (2019). DOI 10.3390/en12071272.
- [19] Tiller, Michael. *Introduction to physical modeling with Modelica*. Springer Science & Business Media (2001).
- [20] Bals, Johann, Ji, Yang, Kuhn, Martin R and Schallert, Christian. "Model based design and integration of more electric aircraft systems using modelica." *Moet forum at European power electronics conference and exhibition*: pp. 1–12, 2009.
- [21] Podlaski, Meaghan, Vanfretti, Luigi, Khare, Abhijit, Nademi, Hamed, Ansell, Phillip, Haran, Kiruba and Balachandran, Thanatheepan. "Initial steps in modeling of CHEETA hybrid propulsion aircraft vehicle power systems using modelica." 2020 AIAA/IEEE Electric Aircraft Technologies Symposium (EATS): pp. 1–16. 2020. IEEE.
- [22] de Castro Fernandes, Marcelo, Wang, Yebin, Wang, Hongyu, Liu, Dehong, Bortoff, Scott A., Vanfretti, Luigi and Takegami, Tomoki. "Modeling, Simulation and Control of Turboelectric Propulsion Systems for More Electric Aircrafts using Modelica." AIAA AVIATION 2022 Forum. 2022. American Institute of Aeronautics and Astronautics. DOI 10.2514/6.2022-3873.
- [23] OpenModelica Association. *OpenModelica User's Guide*, Version 4.0.0 (2023). URL https://openmodelica.org/doc/OpenModelicaUsersGuide/1.21/.
- [24] ARTS-Lab. "Physics-based Prediction of Remaining Useful Life of Lithium-ion Batteries in Fuel Cell-battery Hybrid Aircraft Using an Open-source Modelica Framework." GitHub (2025). URL https://github.com/ARTS-Laboratory/Paper-2025-Physics-based-Prediction-of-Remaining-Useful-Life.
- [25] ARTS-Lab. "Open Modelica modeling of battery fuel cell electric aircraft." GitHub. URL https://github.com/ARTS-Laboratory/Open-Modelica-modeling-of-battery-fuel-cell-electric-aircraft.
- [26] Larminie, James and Dicks, Andrew. *Fuel Cell Systems Explained*. John Wiley & Sons Ltd. (2003).

- [27] Laurencelle, F., Chahine, R., Hamelin, J., Agbossou, K., Fournier, M., Bose, T. K. and Laperrière, A. "Characterization of a Ballard MK5-E Proton Exchange Membrane Fuel Cell Stack." *Fuel Cells* Vol. 1 No. 1 (2001): pp. 66–71. DOI https://doi.org/10.1002/1615-6854(200105)1:1<66::AID-FUCE66>3.0.CO;2-3.
- [28] M., Souleman Njoya, Tremblay, Olivier and Dessaint, Louis-A. "A generic fuel cell model for the simulation of fuel cell vehicles." 2009 IEEE Vehicle Power and Propulsion Conference: pp. 1722–1729. 2009. DOI 10.1109/VPPC.2009.5289692.
- [29] Kim, Junbom, Lee, Seong-Min, Srinivasan, Supramaniam and Chamberlin, Charles E. "Modeling of Proton Exchange Membrane Fuel Cell Performance with an Empirical Equation." *Journal of The Electrochemical Society* Vol. 142 No. 8 (1995): p. 2670. DOI 10.1149/1.2050072. URL https://dx.doi.org/10.1149/1.2050072.
- [30] Hughes, Baker. Masoneilan Control Valve Sizing Handbook, Version Rev. C (2022).
- [31] Samsung SDI Co., Ltd. "Lithium-ion rechargeable cell for power tools Model name: INR18650-30Q." (2014).
- [32] ARTS-Lab. "Dataset electrothermal deformation characterization for Samsung 30Q cell." GitHub (2024). URL https://github.com/ARTS-Laboratory/dataset-electrothermal-deformation-characterization-for-samsung-30Q-cell.
- [33] Chin, C.S., Gao, Z. and Zhang, C.Z. "Comprehensive electro-thermal model of 26650 lithium battery for discharge cycle under parametric and temperature variations." *Journal of Energy Storage* Vol. 28 (2020): p. 101222. DOI 10.1016/j.est.2020.101222.
- [34] Saxena, Saurabh, Hendricks, Christopher and Michael. Pecht, "Cycle life testing and modgraphite/LiCoO2 eling of cells under different state of charge ranges." Journal of Power Sources Vol. 327 (2016): pp. 394–400. DOI https://doi.org/10.1016/j.jpowsour.2016.07.057. URL https://www.sciencedirect.com/science/article/pii/ S0378775316309247.
- [35] "Flight Data." https://www.flightdata.com/ (2024). Accessed: 2024-05-17.
- [36] Fuels, Warter. "Warter Fuels Quality certificate no. 18OBR_IN/A/109, Aviation gasoline AVGAS 100LL." (2018).
- [37] Ma, Yue, Teng, Ho and Thelliez, Marina. "Electro-Thermal Modeling of a Lithium-ion Battery System." *SAE International Journal of Engines* Vol. 3 No. 2 (2010): pp. 306–317. DOI 10.4271/2010-01-2204.